IOP PUBLISHING NANOTECHNOLOGY
Nanotechnology **18** (2007) 295202 (6pp) doi:10.1088/0957-4484/18/29/295202

Impact of oxide substrate on electrical and optical properties of carbon nanotube devices

Yu-Ming Lin, James C Tsang, Marcus Freitag and Phaedon Avouris

IBM T J Watson Research Center, Yorktown Heights, NY 10598, USA

E-mail: yming@us.ibm.com

Received 17 April 2007, in final form 25 May 2007
Published 20 June 2007
Online at stacks.iop.org/Nano/18/295202

Abstract
We have studied suspended nanotube devices to investigate directly the impact of oxide substrate on the properties of nanotubes. The $1/f$ noise amplitude is reduced by about one order of magnitude when the nanotube is suspended, suggesting that the $1/f$ noise is dominated by the trapped charges in the oxide. We have also utilized the enhanced Raman signal intensity in suspended nanotubes to correlate electrical transport properties with Raman spectroscopy on the same individual nanotube, yielding close agreement in the tube diameter determined from both types of experiments.

(Some figures in this article are in colour only in the electronic version)

1. Introduction

Single-wall carbon nanotubes (SWNTs) are excellent realizations of one-dimensional quantum wires [1]. Of particular interest is their potential in nano-electronic applications facilitated by outstanding electrical properties such as the high carrier mobility and current-carrying capability [2–5]. Most electrical experiments of carbon nanotubes have been performed with the nanotubes resting on an oxide surface. Due to the absence of dangling bonds on an ideal nanotube surface, SWNT devices are expected to exhibit similar dc electrical characteristics regardless of the different oxide substrates used. The presence of the oxide substrate, however, may contribute to various non-ideal behaviours and disorder phenomena, such as the device hysteresis and the pronounced current fluctuations, which have been observed in carbon nanotube devices.

The electrical noise in carbon nanotube devices is usually dominated by the $1/f$ noise [6–8] which exhibits a characteristic noise power density approximately proportional to the inverse of frequency. In SWNT devices, the $1/f$ noise is found to be much more pronounced than in conventional bulk devices, and this may seriously limit the potential of nanotubes for applications in electronics. The large $1/f$ noise level in SWNT devices is associated with the small number of carriers in the system [8, 9], and for semiconducting nanotubes the noise amplitude may also be influenced by the Schottky barrier at the contacts [10]. In either case, trapped charges in the oxide have been suggested as one possible source for the $1/f$ noise, where the trapping–detrapping of carriers changes the number of carriers in the channel and also varies the surface potential along the nanotube. While the current fluctuation generated by each trapping–detrapping centre takes the form of random telegraph signal (RTS) [11], the superposition of such RTS noises with a wide distribution of switching time constants yields the $1/f$ noise spectrum. Nevertheless, the contribution of the oxide substrate to the $1/f$ noise has not been determined, the knowledge of which is critical in controlling and lowering the noise level in SWNT devices.

In addition to the implications on electrical fluctuations, the optical transitions in nanotubes, which is a powerful technique to characterize their structure, may also be perturbed by the interaction with the substrate. It is therefore of great importance to study suspended nanotubes that are free from substrate interactions and to probe the intrinsic properties of nanotubes in an unperturbed environment.

Here we investigate the influence of the oxide substrate on the electrical transport and optical properties of SWNT devices by examining the same individual nanotube when lying on the substrate and when being suspended. We find that the $1/f$ noise amplitude is reduced by about one order of magnitude when the nanotube is suspended. This result unambiguously confirms the oxide substrate as the major

source of $1/f$ noise in SWNT devices and provides insight into schemes to reduce the $1/f$ noise in carbon nanotube devices. In addition, the enhanced Raman signal intensity measured from suspended nanotubes allows us to correlate electrical transport measurements with Raman spectroscopy on the same individual nanotube.

2. Experimental results and discussions

Two approaches have often been employed to fabricate suspended nanotube devices. In one approach, nanotubes are grown by chemical vapour deposition (CVD) on a substrate with predefined trenches to form suspended nanotube segments [12]. Alternatively, nanotubes and metal electrodes are first deposited on the substrate, and the substrate between electrodes is subsequently removed by etching [13], leaving suspended nanotubes anchored and supported by electrodes. Here we adopt the latter approach because it allows for the direct comparison of the same nanotube characteristics before and after the oxide substrate is removed.

The fabrication process of suspended nanotube devices in our study is shown schematically in figures 1(a)–(c). Carbon nanotube devices with Pd electrodes are first fabricated on SiO_2 (10 nm)/Si substrates using standard electron-beam lithography and lift-off (see figure 1(a)), as described in [14]. Carbon nanotubes used in our study were synthesized by the arc discharge method, possessing an average diameter of 1.8 nm [15]. A second electron-beam lithography is employed to define the etch window in poly(methyl methacrylate) (PMMA) (see figure 1(b)), followed by brief wet etching of SiO_2 using buffered hydrofluoric (HF) acid. The PMMA layer is then stripped in acetone and the exposed area (not covered by the oxide) is anisotropically etched in 40 wt% KOH solution to a depth of ∼200 nm (see figure 1(c)). The etch is terminated in deionized (DI) water and then transferred to ethanol, followed by drying in N_2. The etch does not attack the Pd metal and carbon nanotubes. Figure 1(d) shows the scanning electron microscopy (SEM) images of two adjacent devices, fabricated on the same individual carbon nanotube, where one of the nanotube segments becomes fully suspended between two metal contacts after the etching process. As shown in figure 1, the isotropic etching of SiO_2 results in undercutting at the nanotube/metal contact and ensures that the oxide has minimal impact on the suspended nanotube device. With this selective etching scheme, we have achieved a high device yield (⩾90%) for producing suspended nanotube segments of lengths below ∼500 nm. As illustrated in figure 1, several devices, both suspended and supported, are fabricated on the same nanotube in order to distinguish reliably the possible variations caused by the etching process from the substrate impact in which we are interested.

Both semiconducting and metallic nanotube devices have been fabricated and studied. Here we first examine and compare the electrical characteristics of semiconducting nanotubes, before and after the etching process. All electrical measurements were performed in vacuum (∼10^{-7} Torr) at room temperature. Figure 2(a) shows the top SEM image of three adjacent devices consisting of one individual semiconducting nanotube and four Pd electrodes, denoted as A, B, C, and D. After the etching, two nanotube segments

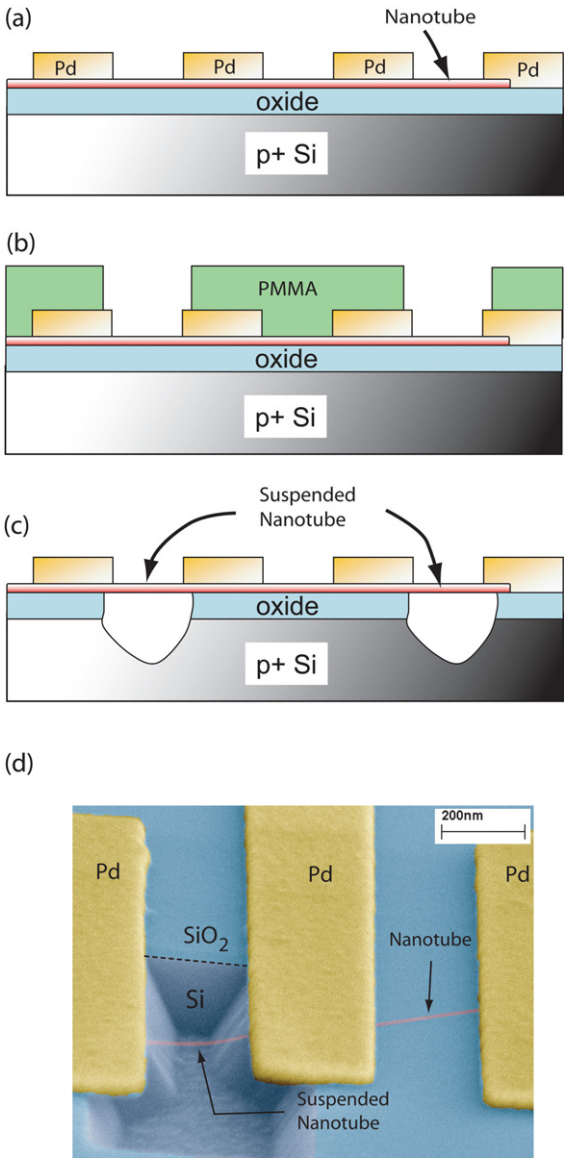

Figure 1. Schematic overview of the fabrication process of suspended carbon nanotube devices. (a) Carbon nanotube devices with Pd metal contacts on a highly p-doped Si substrate and a 10 nm-thick SiO_2 layer. (b) Etch window defined in PMMA for wet etching. (c) Isotropic etching of SiO_2 with buffered HF acid followed by anisotropic etching of Si in KOH solution, resulting in two fully suspended nanotube segments. (d) SEM image showing one fully suspended nanotube device (left) and one regular device (right) on the substrate, both fabricated on a single nanotube.

(AB and CD) become freely suspended while the segment BC remains supported by the substrate. Device BC serves as the control device, and figure 2(b) shows the measured current I as a function of the Si back gate voltage V_g (closed square) and after (open circle) the etching process. The drain bias is kept at −0.5 V. The fact that device BC maintains nearly identical I–V_g characteristics after the process indicates that the etching process (KOH solution) does not affect the contact and oxide quality nor does it introduce structural modifications in the nanotube, which is important in comparing the device characteristics prior to and after etching. Figure 2(c) compares the measured I–V_g curves of device AB before (closed

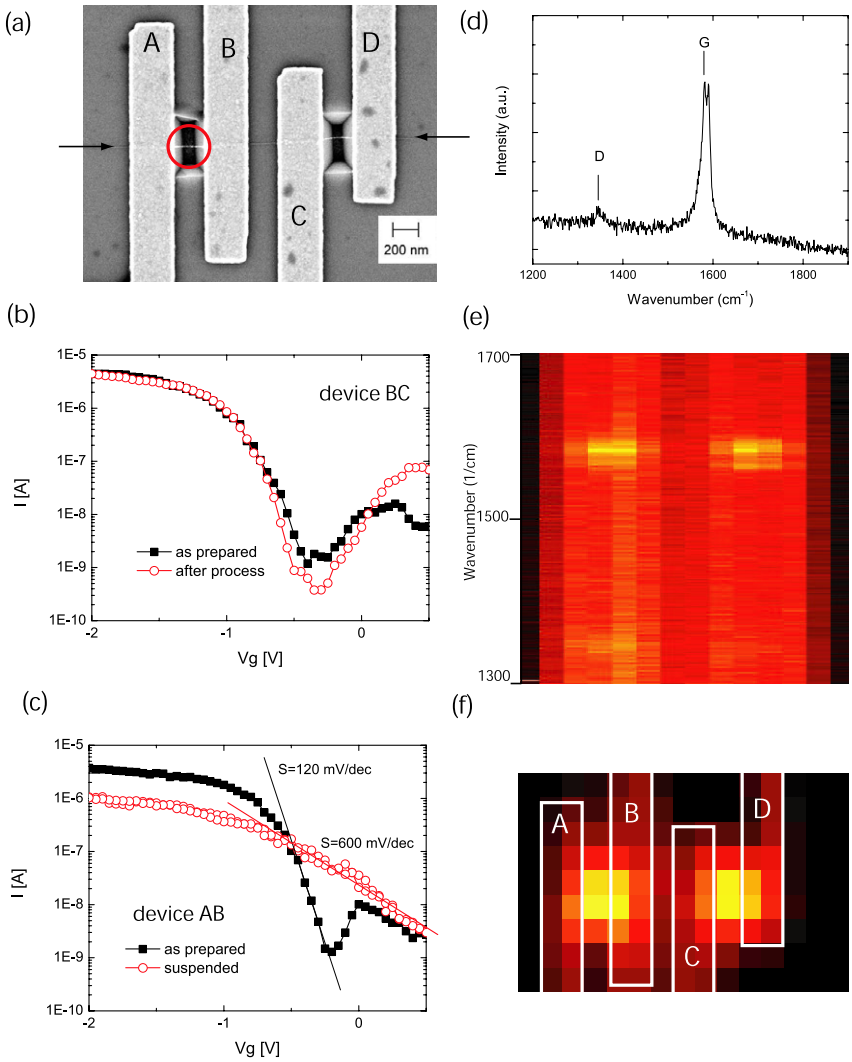

Figure 2. (a) SEM image of the suspended nanotube structure for Raman and electrical measurements. (b) Measured current I as a function of V_g of the nanotube segment between electrodes B and C (device BC), where the nanotube remains supported after etching. The drain voltage is -0.5 V. The device exhibits almost identical electrical characteristics before and after the etching process, indicating that the nanotube itself is not affected or damaged by the process. (c) Measured I–V_g curve at $V_d = -0.5$ V of the nanotube between electrodes A and B (device AB) before and after the removal of the underlying substrate. After being suspended, the device displays a lower on-current and more shallow switching due to the reduced gate control. (d) Raman spectra measured at the suspended nanotube between contacts A and B (circled region in (a)), showing clear G-band and D-band peaks at around 1590 and 1350 cm^{-1}, respectively. (e) Intensity diagram of Raman spectra measured along the nanotube in the area between the two arrows shown in (a). The intensity is plotted as a function of Raman frequency (y-axis) and horizontal position (x-axis), showing enhanced Raman intensity from the suspended nanotube segments. (f) Topographic diagram of the G-band intensity overlayed with the position of Pd electrodes.

square) and after (open circle) the nanotube segment becomes suspended. It is noted that, before etching, both devices AB and BC possess the same on-currents and similar I–V_g characteristics, demonstrating excellent nanotube homogeneity along its length. In figure 2(c), compared with the as-prepared device, the suspended nanotube exhibits a lower on-current and a shallower I–V_g slope due to the weaker gate control from the back gate. The inverse subthreshold slope S of device AB, defined as $(\mathrm{d}\log I/\mathrm{d}V_g)^{-1}$, is increased from 130 mV/dec to ∼600 mV/dec after the trench etching, which is in close agreement with the value of 550 mV/dec extracted from [16] based on an air-gap dielectric of 200 nm.

We also employed Raman spectroscopy to characterize the same suspended nanotube shown in figure 2(a). The probe beam size is about 1 μm with a laser excitation energy of 2.54 eV. Figure 2(d) plots the Raman spectrum taken from the suspended nanotube between electrodes A and B (the circle in figure 2(a)), where a strong G band of tangential modes at around 1590 cm^{-1} and a weak D band activated by defects at $\omega_D = 1350$ cm^{-1} are observed. The Raman signal intensity is found to vary drastically as a function of the beam position. On suspended nanotubes, the measured Raman intensity is significantly stronger (more than ten fold) than the signal from nanotubes lying on the substrate. Figure 2(e) displays the intensity plot of the Raman spectra measured along the nanotube between the two arrows in figure 2(a), showing two bright segments that correspond to the two suspended nanotubes in devices AB and CD. Figure 2(f) shows the

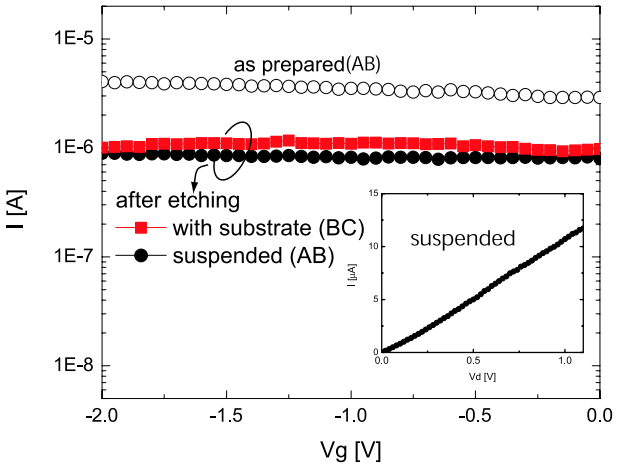

Figure 3. Measured I–V_g curve of metallic nanotube devices at $V_d = -0.1$ V before and after the etching process. The device configuration is the same as that shown in figure 2(a). The inset shows the I–V_d of the suspended nanotube device (device AB), exhibiting the linear response up to 1 V.

Raman image of the entire device obtained by integrating the G-band intensity, where the locations of Pd electrodes are outlined by the white boxes and the bright spots refer to suspended nanotubes. An enhanced Raman signal with a narrower linewidth has also been reported previously for suspended nanotubes [17, 18]. The suppressed Raman signal observed from the nanotubes lying on the substrate is related to the nanotube–substrate interaction that reduces the resonant Raman scattering cross section at our excitation energies.

We utilize the Raman enhancement effect in suspended nanotubes to correlate directly the electrical transport measurements to the structural information obtained from Raman spectroscopy on the same nanotube. As shown in figure 2(d), the G band of a semiconducting nanotube characteristically shows two dominant Lorentzian features, where the high-frequency peak $\omega_G^+ = 1591$ cm^{-1} and the low-frequency peak $\omega_G^- = 1580$ cm^{-1} are associated with vibrations along the nanotube axis and in the circumference direction, respectively. The radial breathing mode (not shown) occurs at $\omega_{RBM} = 126$ cm^{-1}, corresponding to a nanotube diameter of $d_t = 2$ nm, as determined from the relation $\omega_{RBM} = \alpha/d_t$, using $\alpha = 248$ cm^{-1} nm [19]. For a nanotube of 2 nm in diameter, the G-band splitting calculated from the empirical relation $\omega_G^- = \omega_G^+ - c/d_t^2$, where $c = 47.7$ cm^{-1} nm^2 for semiconducting nanotubes [19], yields a frequency difference of 12 cm^{-1}, which is also in good agreement with the measured splitting of 11 cm^{-1}. In a carbon nanotube field-effect transistor (CNFET), the device on-current I_{on} depends on the nanotube diameter and the contact metal, and this dependence has been studied by Chen *et al* [20] for back-gated CNFETs with 10 nm SiO_2 dielectrics and various metal contacts. To compare the on-currents, here we focus on substrate-supported devices that also consist of 10 nm SiO_2 gate oxide and obtain $I_{on} = 3$–4 μA for both devices AB and BC (see figures 2(b) and (c)). For Pd-contacted devices, Chen *et al* have predicted $I_{on} \sim 5$ μA for a 2 nm-diameter nanotube [20], which is in close agreement to the measured on-currents in our devices. Since the nanotube diameter here is independently determined from Raman spectroscopy, these results provide direct experimental support for the dependence of the on-current on the nanotube diameter suggested in [20], which was derived based on statistics.

We next examine the properties of metallic nanotubes using identical device geometry, as shown in figure 2(a), except that the nanotube under investigation is metallic, and the same notations for the electrodes are used. Figure 3 presents the measured I–V_g curves of device AB at $V_d = -0.1$ V before (open circle) and after (closed square) the nanotube segment becomes suspended. As expected for metallic nanotubes, the current is independent of gate voltage in both configurations. After the etching, the neighbouring device BC, where the nanotube remains in contact with the substrate, exhibits a similar current level (closed square in figure 3) to that of suspended nanotube device AB. Some of the suspended nanotube devices possess a slightly higher resistance than that of the as-prepared counterparts, such as the one shown in figure 3. While suspended nanotubes have been reported to exhibit a reduced current-carrying ability with a distinct negative differential conductance behaviour associated with nonequilibrium phonons [21], the reduced current observed in some of our suspended nanotube devices is not likely to be caused by the same origin, but may rather result from the changes in the strain introduced or relaxed during the etching and drying process. One major difference between the two experiments is the length of the suspended nanotube used and the linear I–V behaviour observed in our suspended nanotube devices, as illustrated by the inset of figure 3 showing the the measured current as a function of drain voltage of the suspended nanotube device AB. We note that no negative differential conductance behaviour, which has been reported for suspended nanotubes with channel lengths $\geqslant$600 nm at high currents [21], is observed in our 200 nm-long device up to $V_d = 1$ V. This may be attributed to the more efficient dissipation of hot phonons in a short-channel device, suggesting that short suspended nanotubes may not be subject to the current degradation observed in long suspended nanotubes.

We study the electrical noise of carbon nanotube devices by measuring the current fluctuations at a dc bias. In carbon nanotube devices, the low-frequency current fluctuation is dominated by the $1/f$ noise, which is proportional to the square of the dc current I and can be expressed by $S_I = A_N \times I^2/f$, where A_N is defined as the $1/f$ noise amplitude. Unlike other types of noise, such as thermal noise or shot noise, which are not material-specific properties, A_N generally reflects the sample quality and, most importantly, increases with decreasing device size [22]. Previous studies of carbon nanotube devices have shown a very wide distribution of the noise amplitude A_N, which can span up to five orders of magnitude. For metallic nanotubes, Collins *et al* have shown that the noise amplitude A_N is roughly proportional to the device resistance R [6]. In semiconducting nanotubes, A_N is further modulated by the gate voltage that varies the device resistance, showing an experimental dependence $A_N \sim 1/N$ [23, 9], where N is the number of carriers in the device, in accordance with Hooge's relation [22]. However, even after normalization with the device dimension and resistance, the

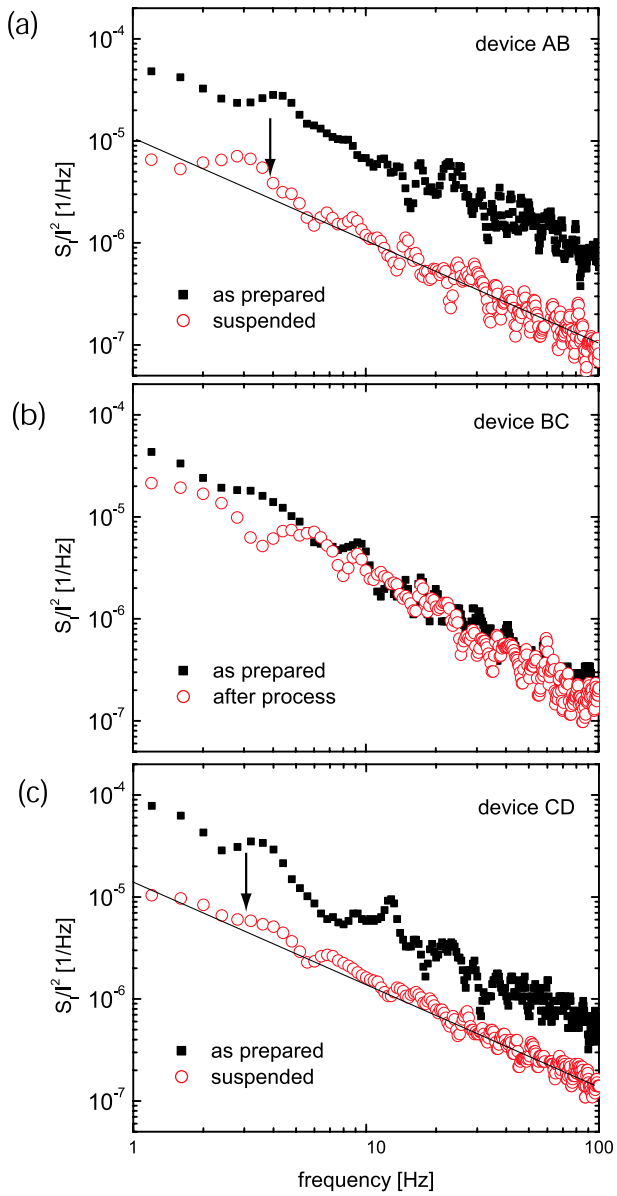

Figure 4. Normalized current noise power spectra S_I/I^2 for three metallic nanotube devices before and after the etching process. The three devices are fabricated on a single carbon nanotube with the same configuration as that shown in figure 2(a), where devices AB and CD consist of suspended nanotubes after the etching process and device BC remains supported. The three devices possess comparable $1/f$ noise levels before etching (black solid squares). After etching, the $1/f$ noise level of suspended nanotube devices (AB and CD) is lowered by about an order of magnitude (red open circles), while the noise level in device BC is unchanged.

noise amplitude A_N in carbon nanotube devices still exhibits significant variation from device to device. Therefore, care must be taken when comparing the noise amplitude between different devices and processes.

In order to illustrate the impact of the oxide substrate on the $1/f$ noise, here we focus on metallic nanotubes where the current remains gate independent both before and after etching. In particular, the devices shown in figure 3 are ideal for the noise study, since the device resistances of the three nanotube segments are similar and remain almost unaffected by the etching process. Figure 4 shows the current power spectra, measured at $V_d = 0.1$ V and normalized by the current square, of three metallic nanotube devices AB, BC, and CD as described above. Before the etching, the current power spectra of these devices (see closed square in figures 4(a)–(c)) all exhibit the f^{-1} dependence with similar A_N values of 6×10^{-5}, 6×10^{-5}, and 8×10^{-5} for devices AB, BC, and CD, respectively. After the etching, the suspended nanotube devices, AB and CD, both show a significantly reduced $1/f$ noise level (open circle in figures 4(a) and (c)) with A_N of 1.2×10^{-5} and 1.0×10^{-5}, respectively. In contrast, the device BC possesses the same $1/f$ noise level after the process (open circle in figure 4(b)). These results unambiguously demonstrate the dominant role played by the oxide substrate with respect to the $1/f$ noise behaviour of carbon nanotube devices. In particular, since the noise level of carbon nanotubes was found to barely vary, within a factor of two, in different gas environments at room temperature [24], the substantial reduction of the noise amplitude in suspended nanotubes here shows that the $1/f$ noise predominately originates from the interaction between the nanotube and the oxide, most likely due to trap charges. It is therefore important to control and improve the oxide quality in order to lower the noise level of carbon nanotube devices. By monitoring the control device (BC), we also show that the etching process in itself does not cause any detectable changes to either dc electrical or noise characteristics in carbon nanotube devices.

3. Conclusion

We have studied suspended nanotube devices to investigate directly the impact of an oxide substrate on the electrical properties of SWNTs. The $1/f$ noise amplitude is significantly reduced by about one order of magnitude when the nanotube is suspended and free from substrate interactions, indicating that the oxide substrate is the major source of $1/f$ noise. We have also utilized the enhanced Raman signal intensity in suspended nanotubes to correlate electrical transport properties with Raman spectroscopy on the same individual nanotube, yielding close agreement in the tube diameters determined from both types of experiments.

Acknowledgments

The authors are indebted to J Appenzeller and Z Chen for their valuable discussions. We also thank B Ek for expert technical assistance.

References

[1] Dresselhaus M S, Dresselhaus G and Avouris Ph 2001 *Carbon Nanotubes: Synthesis, Structure, Properties, and Applications* (Berlin: Springer)
[2] Avouris Ph 2007 *Phys. World* **20** 41–5
[3] Fuhrer M S, Kim B M, Duerkop T and Brintlinger T 2002 *Nano Lett.* **2** 755–9
[4] Yao Z, Kane C L and Dekker C 2000 *Phys. Rev. Lett.* **84** 2941–4
[5] Dai H, Javey A, Pop E, Mann D, Kim W and Lu Y 2006 *ACS Nano* **1** 1–4
[6] Collins P G, Fuhrer M S and Zettl A 2000 *Appl. Phys. Lett.* **76** 894–6

[7] Snow E S, Novak J P, Lay M D and Perkins F K 2004 *Appl. Phys. Lett.* **85** 4172–4
[8] Lin Y-M, Appenzeller J and Avouris Ph 2004 *Nano Lett.* **4** 947–50
[9] Ishigami M, Chen J H, Williams E D, Tobias D, Chen Y F and Fuhrer M S 2006 *Appl. Phys. Lett.* **88** 2031116-1–3
[10] Tersoff J 2007 *Nano Lett.* **7** 194–8
[11] Liu F, Bao M, Kim H-J, Wang K L, Li C, Liu X and Zhou C 2005 *Appl. Phys. Lett.* **86** 163102-1–3
[12] Cao J, Wang Q and Dai H 2005 *Nat. Mater.* **4** 745–9
[13] Nygard J and Cobden D H 2001 *Appl. Phys. Lett.* **79** 4216–8
[14] Lin Y-M, Appenzeller J, Knoch J and Avouris Ph 2005 *IEEE Trans. Nanotechnol.* **4** 481–9
[15] Liu C, Cheng H-M, Cong H T, Li F, Su G, Zhou B L and Dresselhaus M S 2000 *Adv. Mater.* **12** 1190–2
[16] Appenzeller J, Knoch J, Derycke V, Martel R, Wind S and Avouris Ph 2002 *Phys. Rev. Lett.* **89** 126801
[17] Son H, Hori Y, Chou S G, Nezich D, Samsonidze G G, Dresselhaus G, Dresselhaus M S and Rarros E B 2004 *Appl. Phys. Lett.* **85** 4744–6
[18] Kobayashi Y, Yamashita T, Ueno Y, Niwa O, Homma Y and Ogino T 2004 *Chem. Phys. Lett.* **386** 153–7
[19] Dresselhaus M S, Dresselhaus G, Jorio A, Filho A G S and Saito R 2002 *Carbon* **40** 2043–61
[20] Chen Z, Appenzeller J, Knoch J, Lin Y-M and Avouris Ph 2005 *Nano Lett.* **5** 1497–502
[21] Pop E, Mann D, Cao J, Wang Q, Goodson K and Dai H 2005 *Phys. Rev. Lett.* **95** 155505-1–4
[22] Hooge F N 1969 *Phys. Lett.* A **29** 139–40
[23] Lin Y-M, Appenzeller J, Knoch J, Chen Z and Avouris Ph 2006 *Nano Lett.* **6** 930–6
[24] Kingrey D, Khatib O and Collins P G 2006 *Nano Lett.* **6** 1564–8